AIMS Mathematics, 11(11): 38019–38043.
DOI: 10.3934/math.20261469
Received: 13 September 2026
Revised: 02 November 2026
Accepted: 10 November 2026
Published: 16 November 2026

https://www.aimspress.com/journal/Math

Research article

Application of an extended variable-separation technique to the modified Estevez–Mansfield–Clarkson equation in shallow-water and fluid dynamics

Zhi-Hua Bao[1] **and Shami A. M. Alsallami**[2,*]

[1] School of Mathematics and Physics, Hulunbuir University, Hulunbuir, China

[2] Mathematics Department, College of Sciences, Umm Al-Qura University, Makkah 24381, Saudi Arabia

* **Correspondence:** Email: sasallami@uqu.edu.sa.

Abstract: The nonlinear Estevez–Mansfield–Clarkson (EMC) equation is one of the most important nonlinear models in shallow-water hydrodynamics and fluid mechanics. In this paper, two extended variable-separation strategies are applied to the modified (3 + 1)–dimensional EMC equation to obtain several classes of non–traveling wave solutions. In contrast to conventional traveling-wave reductions, the method employed here yields closed-form solutions containing free functions of the independent variables. By imposing distinct constraints on the reduced subsystems, we extract diverse families of explicit exact solutions. Graphical visualizations reveal a wide variety of wave structures. The present technique also offers an efficient route to constructing non-traveling wave solutions to other equations of this type in fluid dynamics.

Keywords: non–traveling solutions; EMC equation; shallow-water models; reduction procedures; closed-form solutions
Mathematics Subject Classification: 35C05, 35C08, 35Q35, 76B15

1. Introduction

Nonlinear dispersive wave equations are crucial mathematical tools for simulating the evolution of long-wave phenomena in various scientific domains. These equations effectively describe ocean waves, tsunamis, and other water–based phenomena in shallow-water hydrodynamics [1–3]. Because of their significance and complexity, many numerical and analytical approaches to nonlinear dispersive wave equations have been developed [4–6].

One of the foundational models in this class was introduced by Boussinesq in 1877 [7]:

$$\psi_{tt} - \psi_{xx} - \gamma\psi_{xxxx} - \beta(\psi^2)_{xx} = 0. \tag{1.1}$$

A variety of higher-order integrable equations were also studied in [8], namely

$$\psi_{tt} - \psi_{xx} - \gamma\psi_{xxxx} - \beta(\psi^2)_{xx} + \alpha\psi_{xt} = 0, \tag{1.2}$$

and

$$\psi_{tt} - \psi_{xx} - \gamma\psi_{xxxx} - \beta(\psi^2)_{xx} + \frac{\alpha^2}{4}\psi_{yy} + \alpha\psi_{yt} = 0. \tag{1.3}$$

Furthermore, the following generalized equation form was studied in [9]:

$$\psi_{tt} - \psi_{xx} + (\psi^n)_{xx} + (\psi^n)_{xxxx} = 0. \tag{1.4}$$

Another example of the (3+1)–dimensional extension of the dispersive wave equations is given in [10]:

$$\psi_{tt} - \psi_{xx} - \beta_1(\psi^2)_{xx} - \beta_2\psi_{xxxx} + \frac{\beta_3^2}{4}\psi_{yy} + \beta_3\psi_{yt} + \beta_4\psi_{xz} = 0. \tag{1.5}$$

Boussinesq-type models describe bidirectional propagation, whereas many coastal problems involve unidirectional propagation over long distances; for these regimes the EMC equation is a suitable model. The (1 + 1)-dimensional EMC equation was first introduced by Mansfield and Clarkson [11] as

$$\psi_{xxxt} + \beta\psi_x\psi_{xt} + \beta\psi_t\psi_{xx} + \psi_{tt} = 0, \tag{1.6}$$

where $\psi = \psi(x, t)$ and β is a constant coefficient. This equation describes the propagation, interaction, and transformation of shallow-water waves. One well-known extension of the EMC equation is expressed as:

$$\left(\psi_x^m\right)_{xxt} + \gamma\left(\psi_x^n\psi_t\right)_x + \psi_{tt} = 0. \tag{1.7}$$

It is worth noting that for $m = n = 1$, Eq (1.7) reduces to the EMC equation (1.6) with $\beta = \gamma$.

To capture more complex physical phenomena, various higher-dimensional extensions of the EMC equation (1.6) have been proposed. For instance, the (2 + 1)-dimensional extension of the model is given by

$$\psi_{yt} + \psi_{xxxy} + \beta\psi_{xx}\psi_y + \beta\psi_x\psi_{xy} = 0. \tag{1.8}$$

Likewise, a (3 + 1)–dimensional modification of (1.6) takes the form

$$\psi_{yt} + \psi_{xxxy} + \beta\psi_{xx}\psi_y + \beta\psi_x\psi_{xy} - \psi_{xz} = 0. \tag{1.9}$$

As established in [11], if ψ is independent of z, Eq (1.9) reduces to Eq (1.8); setting $\psi = u(x, y + t)$ reduces Eq (1.8) to Eq (1.6). Thus, Eqs (1.6) and (1.8) are both reductions of the (3 + 1)–dimensional Eq (1.9). We refer to Eq (1.9) as the modified EMC equation throughout this paper. The EMC equation (1.6) is an important model for studying nonlinear evolution equations and has attracted the attention of many scholars. In [12], the authors studied the model using the modified extended direct algebraic method and the improved (G'/G)-expansion method. The model with the beta-fractional operator was considered in [13] via the modified F-expansion method and the logarithmic transformation. In [14], the authors employed the extended direct algebraic method to extract different soliton solutions to a fractional version of the EMC equation. In addition, using the Riccati-Bernoulli sub-ordinary differential equation (ODE) approach, several exact solutions to the model were reported in [15]. Aliyu et al. systematically derived Lie point symmetries and optimal subalgebras and reduced the model

to ODEs to obtain explicit solutions [16]. In [17], the authors obtained a variety of explicit soliton solutions such as Jacobi elliptic, hyperbolic, trigonometric, and exponential solutions by using the Kumar–Malik method. Further, a generalized $(2+1)$-dimensional form of the EMC equation involving time-dependent coefficients was proposed in [18]. Another time-fractional variant of the model was considered in [19]. Moreover, some symmetries of the $E(m,n)$ equation (1.7) were derived in [20] using the direct reduction method, and classical analytic solutions were compared with extended graph-based PINNs in [21]. Finally, Ceesay et al. [22] obtained the M-shaped wave solutions and multiple breather, periodic lump, and cross-kink wave profiles to the EMC equation by using the Hirota bilinear method.

Many existing solutions to the EMC equation are traveling waves, which inherently restrict the diversity of wave patterns they can describe. The main difference between traveling and non–traveling waves lies in their dynamics. In traveling waves, the speed and the shape of the profiles are fixed; in contrast, the non–traveling waveforms can deform, oscillate, and change shape in a more complicated way as a function of time. This flexibility makes non–traveling waves well-suited to modeling a wide variety of nonlinear problems. Motivated by the need to capture such dynamical behaviors, we employ two variable-separation strategies to construct non–traveling wave solutions to the model. The ansatz used here belongs to the generalized variable-separation approach of [23, 24]. To the best of our knowledge, the technique has not previously been applied to the modified EMC equation (1.9), and the resulting solutions have not been reported before.

The rest of this paper is organized as follows. In Section 2, we apply two extended variable-separation strategies for Eq (1.9). These techniques allow us to reduce the problem to solvable forms. Then, by imposing specific constraint sets, we derive several explicit exact solutions involving trigonometric, hyperbolic, exponential, and rational functions. Section 3 presents the graphical discussion of the exact wave solutions. Finally, some concluding remarks are presented in Section 4.

2. Reduction strategies for Eq (1.9)

In this section, we apply a generalized variable-separation approach [23, 24] within distinct reduction frameworks to derive a wide variety of exact non–traveling solutions to Eq (1.9).

Reduction strategy 1. The first reduction strategy is based on the transformation

$$\psi(x,y,z,t) = p(y,z,t)\cdot\Lambda(\varphi,t) + q(x,y,z,t), \tag{2.1}$$

with the mixed phase variable

$$\varphi = \varepsilon x + \theta(y,z,t), \tag{2.2}$$

in which $\varepsilon \neq 0$ is a constant parameter, and θ is a function to be determined.

Substituting (2.1) into Eq (1.9) and collecting terms according to the order of Λ-derivatives yields the reduced equation

$$\begin{aligned}&\rho_1\frac{\partial\Lambda}{\partial\varphi} + \rho_2 + \rho_4\Lambda + \rho_6\Big(\varepsilon^3\frac{\partial^3\Lambda}{\partial\varphi^3} + \frac{\partial\Lambda}{\partial t}\Big) + \rho_3\rho_7\frac{\partial^2\Lambda}{\partial\varphi^2} + \rho_7\rho_5\Big(\varepsilon^3\frac{\partial^4\Lambda}{\partial\varphi^4} + \frac{\partial^2\Lambda}{\partial\varphi\,\partial t}\Big)\\ &\quad + \varepsilon^2\rho_6\rho_7\Big(\beta\Lambda\frac{\partial^2\Lambda}{\partial\varphi^2} + \beta\Big(\frac{\partial\Lambda}{\partial\varphi}\Big)^2\Big) + 2\beta\varepsilon^2\rho_7^2\rho_5\frac{\partial^2\Lambda}{\partial\varphi^2}\Big(\frac{\partial\Lambda}{\partial\varphi}\Big) = 0,\end{aligned} \tag{2.3}$$

where

$$\begin{aligned}
\rho_1 &= \beta\varepsilon p_y q_x + \beta p\theta_y q_{xx} + \beta\varepsilon p q_{xy} + p_y\theta_t + p\theta_{ty} + \theta_y p_t - \varepsilon p_z,\\
\rho_2 &= q_{ty} + q_{xxxy} - q_{xz} + \beta q_x q_{xy} + \beta q_{xx} q_y,\\
\rho_3 &= \beta\varepsilon\theta_y q_x + \beta\varepsilon^2 q_y + \theta_y\theta_t - \varepsilon\theta_z,\\
\rho_4 &= \beta p_y q_{xx} + p_{ty}, \qquad \rho_5 = \theta_y, \qquad \rho_6 = p_y, \qquad \rho_7 = p.
\end{aligned} \tag{2.4}$$

Equations (2.3) and (2.4) form the basis for the strategy built on ansatz (2.1). Imposing specific constraint sets on $\rho_1, \rho_2, \ldots, \rho_7$ results in solvable reduced equations for Λ and explicit expressions for q and θ.

Case 1.1: Linear wave solution

Imposing the constraint set $\rho_3 = \rho_7 = 1$ and $\rho_1 = \rho_2 = \rho_4 = \rho_5 = \rho_6 = 0$ on Eq (2.3) admits the solution:

$$\Lambda(\varphi, t) = h_1(t)\,\varphi + h_2(t), \tag{2.5}$$

where the h_i are arbitrary functions.

Furthermore, Eq (2.4) under these restrictions gives:

$$\begin{aligned}
&p(y,z,t) = 1,\\
&q(x,y,z,t) = -\beta\int G_1(z,t)\frac{\partial g_1(z,t)}{\partial t}\,dz + g_3\left(\beta G_1(z,t) + x, t\right)\\
&\qquad\qquad + \left(\beta G_1(z,t) + x\right)\int \frac{\partial g_1(z,t)}{\partial t}\,dz + g_1(z,t)y - G_2(z,t),\\
&\theta(y,z,t) = \varepsilon\beta G_1(z,t) - \frac{z}{\varepsilon} + g_4(t),
\end{aligned} \tag{2.6}$$

where $G_i(z,t) = \int g_i(z,t)\,dz$. The corresponding exact non-traveling linear wave solution is:

$$\begin{aligned}
\psi_1(x,y,z,t) = h_1(t)\left(\varepsilon x + \varepsilon\beta G_1(z,t) - \frac{z}{\varepsilon} + g_4(t)\right) + h_2(t) - \beta\int G_1(z,t)\frac{\partial g_1(z,t)}{\partial t}\,dz\\
+ g_3\left(\beta G_1(z,t) + x, t\right) + \left(\beta G_1(z,t) + x\right)\int \frac{\partial g_1(z,t)}{\partial t}\,dz + g_1(z,t)y - G_2(z,t).
\end{aligned} \tag{2.7}$$

Remark 1. Unless stated otherwise, each g_i and each h_i denotes an arbitrary smooth function of its arguments. This freedom allows the wave profile to be modulated independently at different values of y, z, and t, so the solutions need not be traveling waves.

In Figure 1, we present several three-dimensional profiles of the analytic wave solution $\psi_1(x,y,z,t)$ for the (3 + 1)–dimensional EMC equation, with the parameters set to $\varepsilon = 1$ and $\beta = 1$. The remaining set of seed functions $h_1(t)$, $h_2(t)$, $g_1(z,t)$, $g_2(z,t)$, $g_3(\xi,t)$, and $g_4(t)$ is specified for the following three cases: **(a) The Gaussian envelope profile:**

$$\begin{aligned}
&h_1(t) = 0.2e^{-0.1t^2}, \quad h_2(t) = 0.1\sin(0.5t)e^{-0.05t^2}, \quad g_4(t) = 0.5e^{-0.1t^2},\\
&g_1(z,t) = e^{-0.1z^2}\cos(0.5t), \quad g_2(z,t) = ze^{-0.1z^2}\sin(0.3t), \quad g_3(\xi,t) = 0.2e^{-0.05\xi^2}\cos(0.5t).
\end{aligned} \tag{2.8}$$

(b) Multi-peak hyperbolic sech profile:

$$\begin{aligned} &h_1(t) = 0.2\,\mathrm{sech}(0.3t), \quad h_2(t) = 0.1\,\mathrm{sech}^2(0.2t), \quad g_4(t) = 0.5\,\mathrm{sech}(0.3t),\\ &g_1(z,t) = \mathrm{sech}^2(0.3z)\cos(0.4t), \quad g_2(z,t) = \mathrm{sech}(0.3z)\tanh(0.3z)\sin(0.4t),\\ &g_3(\xi,t) = 0.2\,\mathrm{sech}(0.2\xi)\sin(0.3t). \end{aligned} \tag{2.9}$$

(c) Algebraic rational profile:

$$\begin{aligned} &h_1(t) = \frac{0.3}{1+0.1t^2}, \quad h_2(t) = \frac{0.1\cos(0.5t)}{1+0.1t^2}, \quad g_4(t) = \frac{0.4}{1+0.1t^2},\\ &g_1(z,t) = \frac{1-0.1z^2}{(1+0.1z^2)^2}\cos(0.3t), \quad g_2(z,t) = \frac{z\sin(0.3t)}{(1+0.1z^2)^2}, \quad g_3(\xi,t) = \frac{0.2\sin(0.4t)}{1+0.05\xi^2}. \end{aligned} \tag{2.10}$$

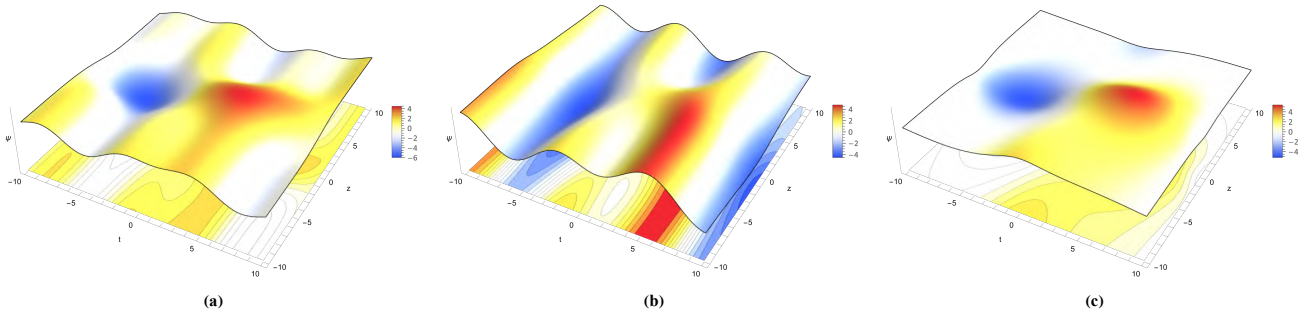


Figure 1. Three-dimensional surface profiles with floor-projected 2D contour maps depicting the localized dynamics of $\psi_1(x,y,z,t)$ evaluated at fixed cross-sections $x = 1$ and $y = 1$ over $t, z \in [-10, 10]$ across: (a) the Gaussian envelope regime, (b) multi-peak hyperbolic sech regime, and (c) algebraic rational profile.

Case 1.2: Parabolic-exponential wave solution

Alternatively, enforcing $\rho_7 = 1$ and setting $\rho_1, \rho_2, \rho_4, \rho_5, \rho_6$ to zero yields the same linear form for $\Lambda(\varphi, t)$ as given in Eq (2.5). Moreover, considering these conditions in Eq (2.4) provides:

$$\begin{aligned} &p(y,z,t) = 1,\\ &q(x,y,z,t) = \frac{1}{2}g_1'(t)x^2 + x\,g_2(z,t) + e^{-\beta g_1(t)}\left(y\int e^{\beta g_1(t)}\frac{\partial g_2}{\partial z}\,dt + \int e^{\beta g_1(t)}g_3(z,t)\,dt + g_4(y,z)\right),\\ &\theta(y,z,t) = g_5(z,t). \end{aligned} \tag{2.11}$$

Through direct substitution, we obtain the parabolic-exponential non–traveling wave solution $\psi_2(x,y,z,t)$ given by

$$\begin{aligned} \psi_2(x,y,z,t) = {} & h_1(t)\,(\varepsilon x + g_5(z,t)) + h_2(t) + \frac{1}{2}g_1'(t)x^2 + x\,g_2(z,t)\\ & + e^{-\beta g_1(t)}\left[y\int e^{\beta g_1(t)}\frac{\partial g_2(z,t)}{\partial z}\,dt + \int e^{\beta g_1(t)}g_3(z,t)\,dt + g_4(y,z)\right]. \end{aligned} \tag{2.12}$$

To illustrate distinct spatiotemporal behaviors (Figure 2), we fix $\varepsilon = 1$ and $\beta = 1$. We also take $g_1(t) = 0.1t$ and consider three sets of the remaining seed functions:

(a) Gaussian–envelope profile:

$$\begin{aligned} &h_1(t) = 0.2e^{-0.1t^2}, \quad h_2(t) = 0.1\cos(0.5t)e^{-0.05t^2}, \\ &g_2(z,t) = e^{-0.1z^2}\sin(0.5t), \quad g_3(z,t) = e^{-0.1z^2}\cos(0.3t), \\ &g_4(y,z) = 0.2e^{-0.1(y^2+z^2)}, \quad g_5(z,t) = 0.5e^{-0.1z^2}\cos(0.5t). \end{aligned} \tag{2.13}$$

(b) Multi-peak hyperbolic–sech profile:

$$\begin{aligned} &h_1(t) = 0.2\,\mathrm{sech}(0.3t), \quad h_2(t) = 0.1\,\mathrm{sech}^2(0.2t), \\ &g_2(z,t) = \mathrm{sech}^2(0.3z)\sin(0.4t), \quad g_3(z,t) = \mathrm{sech}(0.3z)\tanh(0.3z)\cos(0.4t), \\ &g_4(y,z) = 0.2\,\mathrm{sech}(0.2y)\mathrm{sech}(0.2z), \quad g_5(z,t) = 0.5\,\mathrm{sech}(0.3z)\cos(0.4t). \end{aligned} \tag{2.14}$$

(c) Algebraic rational profile:

$$\begin{aligned} &h_1(t) = \frac{0.3}{1+0.1t^2}, \quad h_2(t) = \frac{0.1\sin(0.5t)}{1+0.1t^2}, \\ &g_2(z,t) = \frac{1-0.1z^2}{(1+0.1z^2)^2}\sin(0.3t), \quad g_3(z,t) = \frac{z\cos(0.3t)}{(1+0.1z^2)^2}, \\ &g_4(y,z) = \frac{0.2}{1+0.05y^2+0.05z^2}, \quad g_5(z,t) = \frac{0.4\cos(0.3t)}{1+0.1z^2}. \end{aligned} \tag{2.15}$$

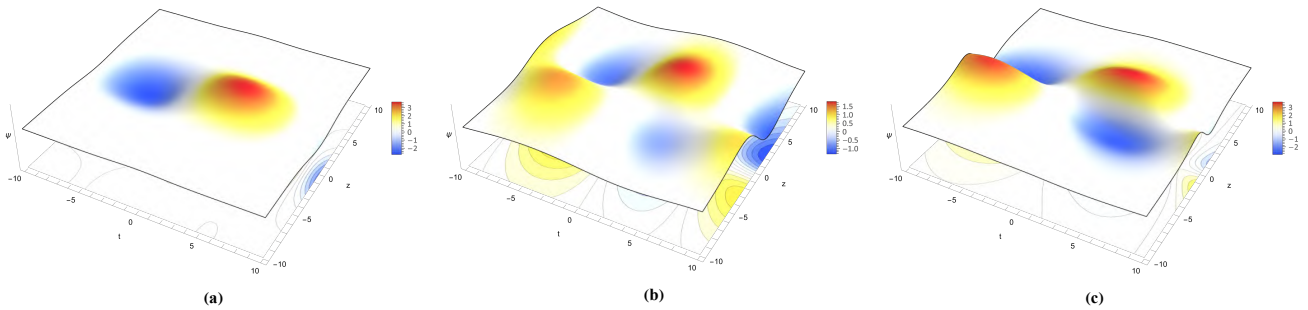


Figure 2. Three-dimensional surface structures with floor-projected 2D contour maps of $\psi_2(x,y,z,t)$ evaluated at cross-sections $x = 1$ and $y = 1$ over $t, z \in [-10, 10]$ for: (a) Gaussian–envelope profile, (b) the multi-peak hyperbolic sech regime, and (c) the algebraic rational seed profile.

Case 1.3: Quadratic spatial background solution

By selecting $\rho_2 = \rho_3$ and $\rho_7 = 1$, while setting the remaining coefficients $\rho_1, \rho_4, \rho_5, \rho_6$ to zero, Eq (2.3) admits the solution:

$$\Lambda(\varphi, t) = -\frac{\varphi^2}{2} + h_1(t)\,\varphi + h_2(t). \tag{2.16}$$

Substituting these constraints into Eq (2.4) yields:

$$\begin{aligned} &p(y,z,t) = 1, \\ &q(x,y,z,t) = \frac{1}{2}g_2'(t)x^2 + g_3(z,t)x \\ &\qquad + \mathrm{e}^{\beta\left(t\varepsilon^2 - g_2(t)\right)}\left[g_5(y,z) - \int \mathrm{e}^{\beta\left(g_2(t) - t\varepsilon^2\right)}\left(\left(\frac{\partial g_1}{\partial z}\varepsilon - \frac{\partial g_3}{\partial z}\right)y - g_4(z,t)\right)dt\right], \\ &\theta(y,z,t) = g_1(z,t). \end{aligned} \tag{2.17}$$

Taking these conditions into account, we obtain the exact non–traveling wave solution with a quadratic spatial background:

$$\begin{aligned} \psi_3(x,y,z,t) = &-\frac{(\varepsilon x + g_1(z,t))^2}{2} + h_1(t)(\varepsilon x + g_1(z,t)) + h_2(t) + \frac{1}{2}g_2'(t)x^2 + g_3(z,t)x \\ &+ \mathrm{e}^{\beta\left(t\varepsilon^2 - g_2(t)\right)}\left[g_5(y,z) - \int \mathrm{e}^{\beta\left(g_2(t) - t\varepsilon^2\right)}\left(\left(\frac{\partial g_1}{\partial z}\varepsilon - \frac{\partial g_3}{\partial z}\right)y - g_4(z,t)\right)dt\right]. \end{aligned} \tag{2.18}$$

We set $g_2(t) = (\varepsilon^2 + c)t$ with $c = 0.1$ and take $\varepsilon = 1, \beta = 1$ and $x = 1, y = 1$; with these parameter values, Figure 3 depicts the behavior of the solution ψ_3 for the following three profiles:

(a) The Gaussian-modulated profile:

$$\begin{aligned} &h_1(t) = 1.2e^{-0.1t^2}, \quad h_2(t) = 0.3\sin(0.6t)e^{-0.08t^2}, \quad g_1(z,t) = 0.5e^{-0.15z^2}\cos(0.4t), \\ &g_3(z,t) = 0.4ze^{-0.15z^2}\sin(0.4t), \quad g_4(z,t) = 0.4e^{-0.15z^2}\cos(0.3t), \quad g_5(y,z) = 0.8e^{-0.1(y^2+z^2)}. \end{aligned} \tag{2.19}$$

(b) The sech-type profile:

$$\begin{aligned} &h_1(t) = \operatorname{sech}(0.2t), \quad h_2(t) = 0.2\operatorname{sech}^2(0.2t), \quad g_1(z,t) = 0.3\operatorname{sech}^2(0.3z)\sin(0.4t), \\ &g_3(z,t) = 0.5\operatorname{sech}(0.3z)\cos(0.4t), \quad g_4(z,t) = 0.3\operatorname{sech}(0.3z)\sin(0.2t), \\ &g_5(y,z) = 0.5\operatorname{sech}(0.2y)\operatorname{sech}(0.2z). \end{aligned} \tag{2.20}$$

(c) The rational profile:

$$\begin{aligned} &h_1(t) = \frac{1.2}{1+0.1t^2}, \quad h_2(t) = \frac{0.2\cos(0.4t)}{1+0.05t^2}, \quad g_1(z,t) = \frac{0.6\cos(0.3t)}{1+0.15z^2}, \\ &g_3(z,t) = \frac{0.4z\sin(0.3t)}{(1+0.15z^2)^2}, \quad g_4(z,t) = \frac{0.3\cos(0.2t)}{1+0.15z^2}, \quad g_5(y,z) = \frac{0.8}{1+0.1y^2+0.1z^2}. \end{aligned} \tag{2.21}$$

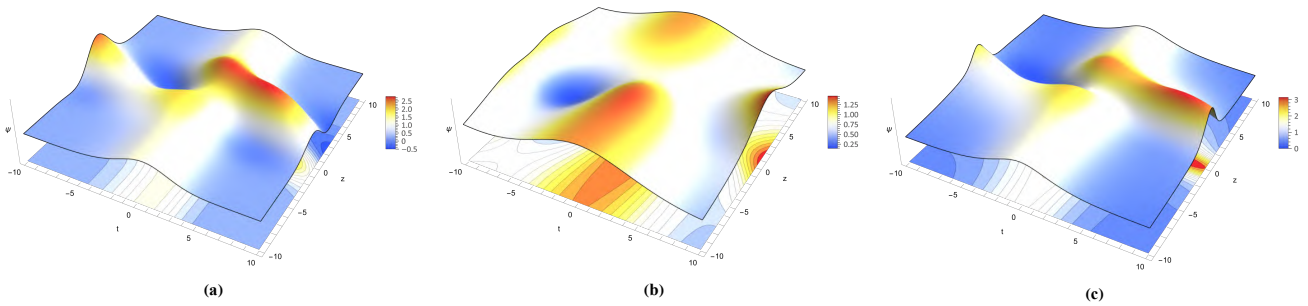


Figure 3. Surface and contour plots of $\psi_3(1, 1, z, t)$ for $(z, t) \in [-10, 10]^2$, with $\varepsilon = \beta = 1$, $c = 0.1$, and $g_2(t) = (\varepsilon^2 + c)t$. Seed functions: (a) Eq (2.19) (Gaussian-modulated), (b) Eq (2.20) (sech-type), (c) Eq (2.21) (rational).

In each panel, the localized part is centered near $t = 0$ and decays in $|z|$. The surfaces are not symmetric in t because of the factor $e^{-\beta ct}$.

Case 1.4: Non–traveling quadratic wave structure

Applying the conditions $\rho_2 = \rho_7$ and $\rho_3 = 1$, alongside $\rho_1 = \rho_4 = \rho_5 = \rho_6 = 0$, transforms Eq (2.3) into the same quadratic form for $\Lambda(\varphi, t)$ as given in Eq (2.16). However, this choice alters the parameter relations in Eq (2.4) to:

$$\begin{aligned} &p\,(y, z, t) = g_2\,(t)\,, \\ &q\,(x, y, z, t) = \left(-g_2\,(t)\,z + \frac{1}{\varepsilon\beta}\frac{\partial g_1}{\partial t}\right)x + \left(\frac{1}{\varepsilon\beta}\frac{\partial g_1}{\partial z} + \frac{1}{\varepsilon^2\beta}\right)y + \int g_3\left(\frac{x\,\varepsilon^2 + g_1\,(z, t)\,\varepsilon + z}{\varepsilon^2}, t\right)dx + g_4\,(z, t)\,, \\ &\theta\,(y, z, t) = g_1\,(z, t)\,. \end{aligned} \tag{2.22}$$

Under these conditions, we obtain the following non–traveling quadratic wave structure:

$$\begin{aligned} \psi_4(x, y, z, t) = {} & g_2(t)\left[-\frac{(\varepsilon x + g_1(z, t))^2}{2} + h_1(t)(\varepsilon x + g_1(z, t)) + h_2(t)\right] \\ & + \left(-g_2\,(t)\,z + \frac{1}{\varepsilon\beta}\frac{\partial g_1}{\partial t}\right)x + \left(\frac{1}{\varepsilon\beta}\frac{\partial g_1}{\partial z} + \frac{1}{\varepsilon^2\beta}\right)y + \int g_3\left(\frac{x\,\varepsilon^2 + g_1\,(z, t)\,\varepsilon + z}{\varepsilon^2}, t\right)dx + g_4\,(z, t)\,, \end{aligned} \tag{2.23}$$

Case 1.5: Linear-modulated wave profile

If we impose $\rho_1 = \rho_2$ and $\rho_3 = \rho_7$, with $\rho_4 = \rho_5 = \rho_6 = 0$, the reduced equation gives:

$$\Lambda\,(\varphi, t) = -\varphi + h_1\,(t)\,. \tag{2.24}$$

Inserting these parameter choices into Eq (2.4) results in:

$$\begin{aligned} p(y,z,t) &= \frac{\partial g_2(z,t)}{\partial z}, \\ q(x,y,z,t) &= \int g_3\left(x+\frac{g_1(z,t)}{\varepsilon}+\frac{g_2(z,t)}{\varepsilon^2},t\right)dx + g_4(z,t) \\ &\quad + x\left(\varepsilon\frac{\partial g_2(z,t)}{\partial z}+\frac{1}{\beta\varepsilon}\frac{\partial g_1(z,t)}{\partial t}+\frac{1}{\beta\varepsilon^2}\frac{\partial g_2(z,t)}{\partial t}\right)+\frac{y}{\beta\varepsilon^2}\left(\frac{\partial g_2(z,t)}{\partial z}+\varepsilon\frac{\partial g_1(z,t)}{\partial z}\right), \\ \theta(y,z,t) &= g_1(z,t). \end{aligned} \tag{2.25}$$

From these auxiliary equations, we formulate the linear-modulated wave profile:

$$\begin{aligned} \psi_5(x,y,z,t) &= \frac{\partial g_2(z,t)}{\partial z}(h_1(t)-g_1(z,t))+\frac{1}{\beta\varepsilon}\left[x\left(\frac{1}{\varepsilon}\frac{\partial g_2(z,t)}{\partial t}+\frac{\partial g_1(z,t)}{\partial t}\right)+y\left(\frac{1}{\varepsilon}\frac{\partial g_2(z,t)}{\partial z}+\frac{\partial g_1(z,t)}{\partial z}\right)\right] \\ &\quad + \int g_3\left(x+\frac{g_1(z,t)}{\varepsilon}+\frac{g_2(z,t)}{\varepsilon^2},t\right)dx + g_4(z,t). \end{aligned} \tag{2.26}$$

By assigning specific seed configurations within the reduction framework of Eq (2.26), we obtain distinct localized wave profiles for $\psi_5(x,y,z,t)$ evaluated at $x=1, y=1$ with scaling constants $\varepsilon = 1, \beta = 0.8$ (Figure 4):

(a): Utilizing coupled hyperbolic secant functions for the seed functions $g_1(z,t)$ and $g_2(z,t)$ results in a localized pulse structure centered near the spatiotemporal origin:

$$\begin{aligned} &h_1(t)=1.8\,\mathrm{sech}(0.2t), \quad g_1(z,t)=0.3\,\mathrm{sech}(0.3z)\,\mathrm{sech}(0.2t), \quad g_2(z,t)=0.4\,\mathrm{sech}^2(0.3z)\,\mathrm{sech}(0.2t), \\ &g_3(\xi,t)=0.8\,\mathrm{sech}(0.2t)\,\mathrm{sech}^2(\xi), \quad g_4(z,t)=0.5\,\mathrm{sech}^2(0.3z). \end{aligned} \tag{2.27}$$

(b): Employing Gaussian-weighted harmonic modulations gives:

$$\begin{aligned} &h_1(t)=1.5e^{-0.08t^2}, \quad g_1(z,t)=0.4e^{-0.1z^2}\cos(0.5t), \quad g_2(z,t)=0.3e^{-0.1z^2}\sin(0.5t), \\ &g_3(\xi,t)=e^{-0.08t^2}\cos(0.5t)\,\mathrm{sech}^2(\xi), \quad g_4(z,t)=0.4e^{-0.1z^2}\cos(0.5t). \end{aligned} \tag{2.28}$$

(c): Incorporating rational functions combined with hyperbolic tangent spatial profiles yields:

$$\begin{aligned} &h_1(t)=\frac{1.5}{1+0.08t^2}, \quad g_1(z,t)=\frac{0.5\tanh(0.3z)}{1+0.1t^2}, \quad g_2(z,t)=\frac{0.4\,\mathrm{sech}(0.3z)}{1+0.08t^2}, \\ &g_3(\xi,t)=\frac{0.8}{1+0.08t^2}\,\mathrm{sech}^2(\xi), \quad g_4(z,t)=\frac{0.4\tanh(0.3z)}{1+0.1z^2}. \end{aligned} \tag{2.29}$$

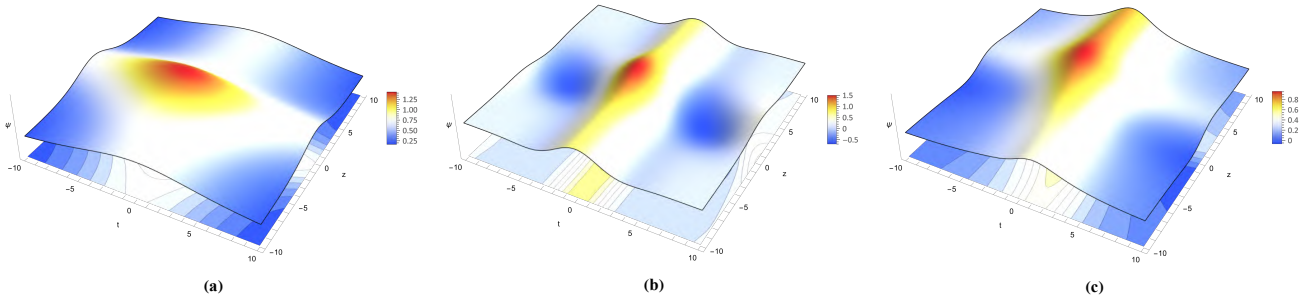


Figure 4. Surface and contour plots of $\psi_5(1, 1, z, t)$ for $(z, t) \in [-10, 10]^2$, with $\varepsilon = 1$ and $\beta = 0.8$. Seed functions: (a) Eq (2.27), (b) Eq (2.28), (c) Eq (2.29).

Figure 4 (a) shows a single localized pulse near the origin. Figures 4 (b) and (c) show ridges that extend along the t-direDction.

Case 1.6: Exponential decay wave structure

Under the constraints $\rho_7 = 1$ and $\rho_1 = \rho_2 = \rho_3$, with $\rho_4 = \rho_5 = \rho_6 = 0$, Eq (2.3) admits the solution

$$\Lambda(\varphi, t) = h_1(t)\, \mathrm{e}^{-\varphi} - \varphi + h_2(t). \tag{2.30}$$

As a result, the auxiliary equations in Eq (2.4) simplify to:

$$\begin{aligned} &p(y, z, t) = 1, \\ &q(x, y, z, t) = g_2(z, t) + \int g_3\left(x + \frac{g_4(z,t)}{\varepsilon}, t\right) dx + \frac{x}{\beta\varepsilon}\left(\frac{\partial g_4(z,t)}{\partial t}\right) + \frac{y}{\beta\varepsilon}\left(\frac{\partial g_4(z,t)}{\partial z}\right), \\ &\theta(y, z, t) = g_4(z, t). \end{aligned} \tag{2.31}$$

Hence, the exponential decay wave structure is expressed as:

$$\begin{aligned} \psi_6(x, y, z, t) = {} & h_1(t)\, \mathrm{e}^{-(\varepsilon x + g_4(z,t))} - (\varepsilon x + g_4(z, t)) + h_2(t) \\ & + g_2(z, t) + \int g_3\left(x + \frac{g_4(z,t)}{\varepsilon}, t\right) dx + \frac{x}{\beta\varepsilon}\left(\frac{\partial g_4(z,t)}{\partial t}\right) + \frac{y}{\beta\varepsilon}\left(\frac{\partial g_4(z,t)}{\partial z}\right). \end{aligned} \tag{2.32}$$

Setting $\beta = 0.65$, we evaluate the solution $\psi_6(x, y, z, t)$ at $x = 1, y = 1$ with $\varepsilon = 1$. Under these conditions, Figure 5 shows the evolution of this solution in the following three sets of seed functions:
(a): Coupling Bessel-type integral kernels with multi-frequency temporal modulations:

$$\begin{aligned} &h_1(t) = 2.5\,\mathrm{sech}(0.15t)\cos(0.8t), \quad h_2(t) = 1.2e^{-0.04t^2}\sin(0.6t), \\ &g_2(z, t) = 0.7\sin(0.4z)\cos(0.5t), \quad g_4(z, t) = 0.6\cos(0.4z)\,\mathrm{sech}(0.2t), \\ &g_3(\xi, t) = 1.4\,\mathrm{sech}(0.15t)\sin(0.7t)J_0(\xi). \end{aligned} \tag{2.33}$$

(b): Employing trigonometric functions within the integral kernel:

$$\begin{aligned} &h_1(t) = 2e^{-0.05t^2}\cos(t), \quad h_2(t) = \mathrm{sech}(0.2t)\cos(0.8t), \\ &g_2(z, t) = 0.8e^{-0.05z^2}\sin(0.8t), \quad g_4(z, t) = 0.65\,\mathrm{sech}(0.3z)\cos(0.6t), \\ &g_3(\xi, t) = 1.5e^{-0.05t^2}\cos(0.9t)\sin^2(\xi). \end{aligned} \tag{2.34}$$

(c): Utilizing rational damping factors combined with hyperbolic sech-tanh compound states:

$$\begin{aligned} h_1(t) &= \frac{2.2}{1+0.03t^2}\cos(0.7t), \quad h_2(t) = \frac{0.9}{1+0.05t^2}\sin(0.5t), \\ g_2(z,t) &= \frac{0.7\tanh(0.3z)\cos(0.5t)}{1+0.04t^2}, \quad g_4(z,t) = \frac{0.6\,\mathrm{sech}(0.3z)\sin(0.5t)}{1+0.04t^2}, \\ g_3(\xi,t) &= \frac{1.3}{1+0.03t^2}\cos(0.6t)\tanh(\xi)\,\mathrm{sech}(\xi). \end{aligned} \tag{2.35}$$

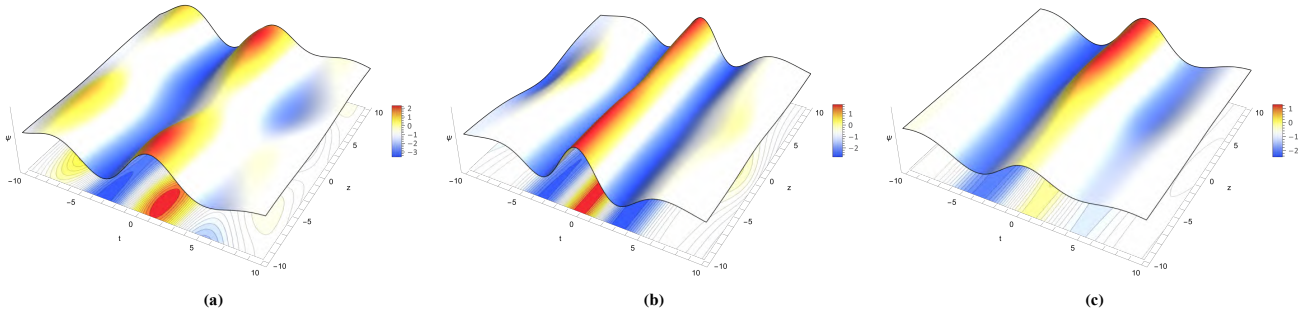


Figure 5. Surface and contour plots of $\psi_6(1,1,z,t)$ for $(z,t) \in [-10,10]^2$, with $\varepsilon = 1$ and $\beta = 0.65$. Seed functions: (a) Eq (2.33), (b) Eq (2.34), (c) Eq (2.35).

The $\cos(0.4z)$ and $\sin(0.4z)$ terms produce a periodic structure in z. The time factors modulate its amplitude and phase.

Case 1.7: Exponentially decaying phase solution

For $\rho_1 = \rho_5 = \rho_7 = 1$ and $\rho_2 = \rho_4 = \rho_6 = 0$, Eq (2.3) gives:

$$\Lambda(\varphi,t) = c\,\varphi\,\mathrm{e}^{-t}. \tag{2.36}$$

Furthermore, solving the constraint system outlined in Eq (2.4) provides:

$$\begin{aligned} &p(y,z,t) = 1, \\ &q(x,y,z,t) = \frac{\mathrm{e}^{2z/\varepsilon}}{2D}x^2 + \frac{g_1(\tau)}{\beta\varepsilon D}xy + x\,g_2(z,t) + g_3(z,t) + \mathrm{e}^{-S}\Big[g_4(y,z) + \int \mathrm{e}^{S}\Big(y\,\Phi_0 + \tfrac{1}{2}y^2\,\Phi_1\Big)dt\Big], \\ &\theta(y,z,t) = y + g_5(z,t), \end{aligned} \tag{2.37}$$

where

$$\begin{aligned} &\tau = t - \frac{z}{\varepsilon}, \qquad D = \beta\mathrm{e}^{2z/\varepsilon} + g_1(\tau), \qquad S = \beta\mathrm{e}^{2z/\varepsilon}\int\frac{dt}{D}, \\ &\Phi_0 = \frac{\partial g_2}{\partial z} - \frac{g_1(\tau)\,g_2}{\varepsilon D}, \qquad \Phi_1 = -\frac{g_1^2(\tau) + \beta\mathrm{e}^{2z/\varepsilon}(2g_1(\tau) + g_1'(\tau))}{\beta\varepsilon^2 D^2}. \end{aligned} \tag{2.38}$$

Under these conditions, provided that $D \neq 0$, we obtain the following exact non–traveling wave solution:

$$\psi_7(x,y,z,t) = c\,\mathrm{e}^{-t}(\varepsilon x + y + g_5(z,t)) + q(x,y,z,t), \tag{2.39}$$

where q is given by (2.37).

Case 1.8: Exponential linear-background solution

Under the constraints $\rho_1 = \rho_7$, $\rho_3 = 1$, and $\rho_2 = \rho_4 = \rho_5 = \rho_6 = 0$, we obtain

$$\Lambda(\varphi, t) = h_1(t) + h_2(t)\, \mathrm{e}^{-\varphi}. \tag{2.40}$$

Solving for p, q, and θ gives

$$\begin{aligned} p(y,z,t) &= g_4(t)\, \mathrm{e}^{-\frac{z}{\varepsilon}}, \\ q(x,y,z,t) &= -\beta \int G_1(z,t) \left(\frac{\partial}{\partial t} g_1(z,t)\right) dz + g_3(\beta G_1(z,t) + x, t) \\ &\quad + (x + \beta G_1(z,t)) \int \left(\frac{\partial}{\partial t} g_1(z,t)\right) dz + g_1(z,t)\, y - G_2(z,t), \\ \theta(y,z,t) &= \varepsilon\beta G_1(z,t) - \frac{z}{\varepsilon} + g_5(t). \end{aligned} \tag{2.41}$$

A non–traveling wave solution is then given by:

$$\begin{aligned} \psi_8(x,y,z,t) = g_4(t)\, \mathrm{e}^{-\frac{z}{\varepsilon}} \Big[h_1(t) + h_2(t) \exp\left(-\varepsilon x - \varepsilon\beta G_1(z,t) + \frac{z}{\varepsilon} - g_5(t)\right)\Big] \\ - \beta \int G_1(z,t) \left(\frac{\partial}{\partial t} g_1(z,t)\right) dz + g_3(\beta G_1(z,t) + x, t) \\ + (x + \beta G_1(z,t)) \int \left(\frac{\partial}{\partial t} g_1(z,t)\right) dz + g_1(z,t)\, y - G_2(z,t). \end{aligned} \tag{2.42}$$

Case 1.9: An unconstrained functional regime

Finally, setting all coefficients ρ_1 through ρ_6 to zero causes the reduced differential operator in Eq (2.3) to vanish identically for any smooth function. Solving the corresponding system for p, q, and θ gives:

$$\begin{aligned} p(y,z,t) &= g_4(t), \\ q(x,y,z,t) &= g_1(z,t)\, y + \int \left(x \frac{\partial g_1(z,t)}{\partial t} - g_2(z,t)\right) dz + g_3(\beta G_1(z,t) + x, t), \\ \theta(y,z,t) &= \beta\varepsilon G_1(z,t) + g_5(t). \end{aligned} \tag{2.43}$$

This unconstrained functional framework yields a general family of non–traveling solutions, given by:

$$\begin{aligned} \psi_9(x,y,z,t) = & g_4(t)\, \Lambda(\varepsilon x + \beta\varepsilon G_1(z,t) + g_5(t), t) \\ & + g_1(z,t)\, y + \int \left(x \frac{\partial g_1(z,t)}{\partial t} - g_2(z,t)\right) dz + g_3(\beta G_1(z,t) + x, t). \end{aligned} \tag{2.44}$$

Remark 2. It is worth emphasizing that in ψ_9 as given in Eq (2.44), $\Lambda(\varphi, t)$ is no longer restricted by any differential constraints and thus can be chosen as any smooth function. This flexibility, combined with the ability to choose arbitrary functions in q and θ, yields a remarkably rich solution space for the model. However, the profile, amplitude, and time dependence of such solutions arise from the chosen seed functions rather than from the nonlinearity of the model.

In Figure 6, we examine three choices of the seed functions:
(a): The first seed set is characterized by a multi-frequency core profile

$$\Lambda(\varphi, t) = \operatorname{sech}^2(\varphi)\cos(3\varphi)\cos(2t).$$

Moreover, we consider $g_1(z,t) = \operatorname{sech}^2(0.8z)\cos(2t)$, and the remaining seed functions:

$$\begin{aligned} &g_2(z,t) = 0.5\sin(2z)\cos(1.5t)e^{-0.05t^2}, \quad g_3(\xi,t) = 0.4\sin(2\xi)\cos(\xi)\operatorname{sech}(0.1t^2), \\ &g_4(t) = 1.5, \quad g_5(t) = \sin(1.5t). \end{aligned} \tag{2.45}$$

(b): The second seed set is constructed by a high-harmonic core

$$\Lambda(\varphi, t) = \operatorname{sech}(\varphi)\cos(2.5\varphi)\sin(2t),$$

together with a trigonometric envelope $g_1(z,t) = \cos(2z)e^{-0.05t^2}\sin(t)$, and seed functions:

$$\begin{aligned} &g_2(z,t) = 0.6\cos(3z)\sin(t), \quad g_3(\xi,t) = 0.5\cos(2\xi)\operatorname{sech}(0.2t^2), \\ &g_4(t) = 2, \quad g_5(t) = 0.8\cos(t). \end{aligned} \tag{2.46}$$

(c): The third seed set employs the Gaussian-modulated exponential core

$$\Lambda(\varphi, t) = \exp(-0.5\varphi^2)\cos(3\varphi)\cos(1.5t),$$

along with the kernel $g_1(z,t) = \exp(-0.2z^2)\cos(2z)\cos(t)$, and seed functions:

$$\begin{aligned} &g_2(z,t) = 0.4\sin(2.5z)e^{-0.08t^2}, \quad g_3(\xi,t) = 0.6\sin(1.5\xi)\cos(1.5\xi)e^{-0.05t^2}, \\ &g_4(t) = 1.8, \quad g_5(t) = 0.5\sin(2t). \end{aligned} \tag{2.47}$$

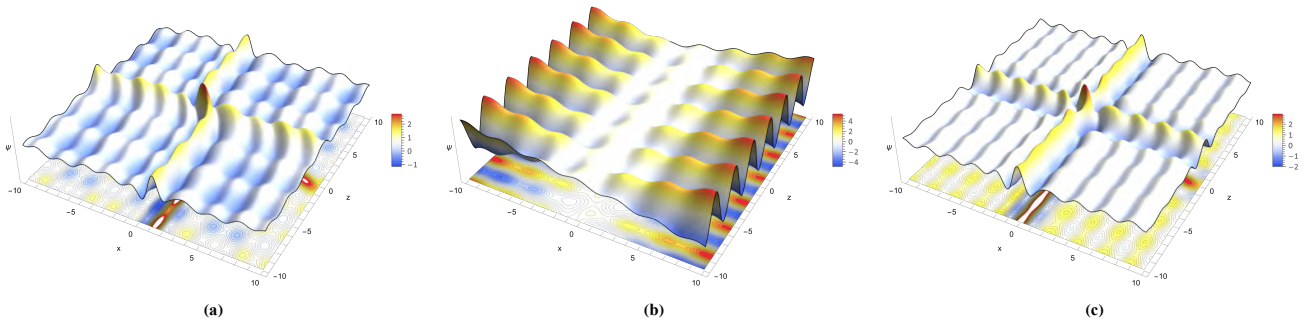


Figure 6. Surface and contour plots of $\psi_9(x, 1, z, 1)$ for $(x, z) \in [-10, 10]^2$, with $\varepsilon = \beta = 1$. Core function Λ and seed functions: (a) Eq (2.45), (b) Eq (2.46), (c) Eq (2.47).

The oscillations come from the $\cos(3\varphi)$ and $\cos(2.5\varphi)$ factors in Λ. The sech and Gaussian factors keep the pattern localized around the curve $\varphi = 0$.

Reduction strategy 2. To obtain additional classes of exact solutions, we now use the ansatz

$$\psi(x, y, z, t) = p(z, t) \cdot \Omega(\varphi, \zeta) + q(y, z, t), \tag{2.48}$$

along with two phase variables

$$\varphi = \varepsilon_1 x + \theta(y,t), \quad \zeta = \varepsilon_2 x + \eta(z,t), \tag{2.49}$$

in which $\varepsilon_1, \varepsilon_2 \neq 0$ are constants, and θ and η are functions to be determined.

Substituting (2.48) into Eq (1.9) and collecting terms according to the order of Ω-derivatives gives

$$\begin{aligned}
&\rho_8\rho_1\frac{\partial^2\Omega}{\partial\varphi\,\partial\zeta} - \varepsilon_2\rho_7\frac{\partial\Omega}{\partial\zeta} + \varepsilon_2\rho_8\rho_4\frac{\partial^2\Omega}{\partial\zeta^2} + \rho_8\rho_3\frac{\partial^2\Omega}{\partial\varphi^2}\\
&+ \rho_6\rho_8\Big(\varepsilon_1^3\frac{\partial^4\Omega}{\partial\varphi^4} + 3\varepsilon_1^2\varepsilon_2\frac{\partial^4\Omega}{\partial\varphi^3\partial\zeta} + 3\varepsilon_1\varepsilon_2^2\frac{\partial^4\Omega}{\partial\varphi^2\partial\zeta^2} + \varepsilon_2^3\frac{\partial^4\Omega}{\partial\varphi\,\partial\zeta^3}\Big) + \beta\rho_6\rho_8^2\Big(\varepsilon_1\varepsilon_2\frac{\partial\Omega}{\partial\zeta}\frac{\partial^2\Omega}{\partial\varphi^2}\\
&+ \varepsilon_2^2\frac{\partial\Omega}{\partial\zeta}\frac{\partial^2\Omega}{\partial\varphi\,\partial\zeta} + 2\varepsilon_1^2\frac{\partial\Omega}{\partial\varphi}\frac{\partial^2\Omega}{\partial\varphi^2} + 3\varepsilon_1\varepsilon_2\frac{\partial\Omega}{\partial\varphi}\frac{\partial^2\Omega}{\partial\varphi\,\partial\zeta} + \varepsilon_2^2\frac{\partial\Omega}{\partial\varphi}\frac{\partial^2\Omega}{\partial\zeta^2}\Big) + \rho_5 + \rho_2\frac{\partial\Omega}{\partial\varphi} = 0,
\end{aligned} \tag{2.50}$$

with the coefficients

$$\begin{aligned}
&\rho_1 = 2q_y\beta\varepsilon_1\varepsilon_2 + \theta_y\eta_t - \eta_z\varepsilon_1, \qquad \rho_2 = p\theta_{ty} + \theta_y p_t - p_z\varepsilon_1,\\
&\rho_3 = q_y\beta\varepsilon_1^2 + \theta_y\theta_t, \qquad \rho_4 = q_y\beta\varepsilon_2 - \eta_z, \qquad \rho_5 = q_{ty}, \qquad \rho_6 = \theta_y, \qquad \rho_7 = p_z, \qquad \rho_8 = p.
\end{aligned} \tag{2.51}$$

By imposing various conditions on the coefficient functions in (2.51), we obtain several simplified systems. Solving these reduced forms yields the following categories:

Case 2.1: Exponential linear-background wave solution

First, let us consider $\rho_4 = 1, \rho_1 = \rho_2 = \rho_5 = \rho_6 = \rho_7 = 0$ in (2.50). Then we obtain:

$$\Omega(\varphi,\zeta) = \Big(c_1 \mathrm{e}^{\frac{2\varepsilon_1\zeta}{\varepsilon_2}} + c_2\Big)\mathrm{e}^{\varphi - \frac{\varepsilon_1}{\varepsilon_2}\zeta} + c_3\zeta. \tag{2.52}$$

Applying these relations to Eq (2.51) yields:

$$p(z,t) = g_1(t), \qquad q(y,z,t) = -\frac{y}{\varepsilon_2\beta} + g_3(z,t), \qquad \theta(y,t) = g_2(t), \qquad \eta(z,t) = -2z + g_4(t). \tag{2.53}$$

Consequently, a wave solution to the model is given by:

$$\begin{aligned}
\psi_{10}(x,y,z,t) =& g_1(t)\Big[c_1\exp\Big(g_2(t) + 2\varepsilon_1 x - \frac{2\varepsilon_1}{\varepsilon_2}z + \frac{\varepsilon_1}{\varepsilon_2}g_4(t)\Big)\\
&+ c_2\exp\Big(g_2(t) + \frac{2\varepsilon_1}{\varepsilon_2}z - \frac{\varepsilon_1}{\varepsilon_2}g_4(t)\Big) + c_3(\varepsilon_2 x - 2z + g_4(t))\Big] - \frac{y}{\varepsilon_2\beta} + g_3(z,t).
\end{aligned} \tag{2.54}$$

Case 2.2: Logistic-type step wave structure

Alternatively, setting $\rho_4 = \rho_6$ and $\rho_1 = \rho_2 = \rho_3 = \rho_5 = 0$ in the reduced system gives:

$$\Omega(\varphi,\zeta) = -\frac{6\varepsilon_1}{\beta}\left(\frac{1}{1+\mathrm{e}^{\varphi}}\right) - \frac{\varepsilon_1^2}{\varepsilon_2\beta}\zeta. \tag{2.55}$$

Using these values in Eq (2.51) gives:

$$p(z,t)=1, \qquad q(y,z,t)=g_2(y)+g_1(z,t), \qquad \theta(y,t)=-\frac{\varepsilon_1^2 t}{\varepsilon_2}+\beta\varepsilon_2 g_2(y), \qquad \eta(z,t)=-2\varepsilon_1 t. \tag{2.56}$$

Consequently, the resulting closed-form expression represents a logistic-type step wave structure:

$$\psi_{11}(x,y,z,t)=-\frac{6\varepsilon_1}{\beta}\left(\frac{1}{1+\exp\left(\varepsilon_1 x-\frac{\varepsilon_1^2 t}{\varepsilon_2}+\beta\varepsilon_2 g_2(y)\right)}\right)-\frac{\varepsilon_1^2}{\varepsilon_2\beta}\left(\varepsilon_2 x-2\varepsilon_1 t\right)+g_2(y)+g_1(z,t). \tag{2.57}$$

Case 2.3: Compound trigonometric lattice solution

Imposing the restrictions $\rho_3=\rho_8$ and $\rho_5=\rho_7$, alongside $\rho_1=\rho_2=\rho_6=0$, transforms the reduced system into:

$$\Omega(\varphi,\zeta)=(c_1\sin(\varphi)+c_2\cos(\varphi))\cos\left(\frac{\varepsilon_1\zeta}{\varepsilon_2}\right)+(c_3\sin(\varphi)+c_4\cos(\varphi))\sin\left(\frac{\varepsilon_1\zeta}{\varepsilon_2}\right). \tag{2.58}$$

Inserting these parameter reductions into Eq (2.51) results in:

$$p(z,t)=1, \qquad q(y,z,t)=\frac{y}{\beta\varepsilon_1^2}+g_2(z,t), \qquad \theta(y,t)=g_1(t), \qquad \eta(z,t)=\frac{2\varepsilon_2 z}{\varepsilon_1^2}+g_3(t). \tag{2.59}$$

Accordingly, the compound trigonometric lattice solution to the model is obtained as:

$$\begin{aligned}\psi_{12}(x,y,z,t)=&\left[(c_1\sin(\varepsilon_1 x+g_1(t))+c_2\cos(\varepsilon_1 x+g_1(t)))\cos\left(\varepsilon_1 x+\frac{2z}{\varepsilon_1}+\frac{\varepsilon_1}{\varepsilon_2}g_3(t)\right)\right.\\&\left.+(c_3\sin(\varepsilon_1 x+g_1(t))+c_4\cos(\varepsilon_1 x+g_1(t)))\sin\left(\varepsilon_1 x+\frac{2z}{\varepsilon_1}+\frac{\varepsilon_1}{\varepsilon_2}g_3(t)\right)\right]+\frac{y}{\beta\varepsilon_1^2}+g_2(z,t).\end{aligned} \tag{2.60}$$

To graphically examine the exact analytic profiles of $\psi_{12}(x,y,z,t)$, we set $\beta=1$, $\varepsilon_1=1$, $\varepsilon_2=1$, $c_1=1$, $c_2=0.5$, $c_3=0.5$, $c_4=1$, and $y=1$, yielding the configurations shown in Figure 7 across the following three sets of seed functions:

(a) Harmonic pattern: Using standard sinusoidal and cosinusoidal phase modulations:

$$g_1(t)=0.5\cos(0.4t), \quad g_2(z,t)=0.4\sin(0.5z)e^{-0.05t^2}, \quad g_3(t)=0.3\sin(0.2t). \tag{2.61}$$

(b) Phase-modulated lattice: Employing hyperbolic secant damping and nonlinear phase coupling to create complex multi-peak structures:

$$g_1(t)=1.5\,\mathrm{sech}(0.3t)\cos(t), \quad g_2(z,t)=1.2\sin(1.5z)\,\mathrm{sech}(0.4z)\cos(0.8t), \quad g_3(t)=\tanh(0.2t). \tag{2.62}$$

(c) Multi-periodic wave lattice: Utilizing coupled harmonic functions and exponential decay factors:

$$g_1(t)=0.8\sin(0.6t), \quad g_2(z,t)=0.6\cos(1.2z)e^{-0.1t^2}, \quad g_3(t)=0.5\cos(0.4t). \tag{2.63}$$

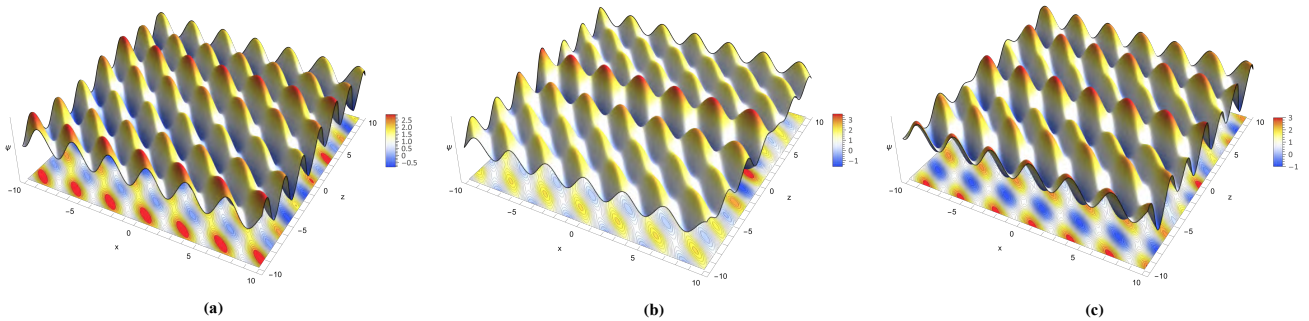


Figure 7. Surface and contour plots of $\psi_{12}(x, 1, z, 1)$ for $(x, z) \in [-10, 10]^2$, with $\beta = \varepsilon_1 = \varepsilon_2 = 1$, $c_1 = 1$, $c_2 = c_3 = 0.5$, and $c_4 = 1$. Seed functions: (a) Eq (2.61) (harmonic pattern), (b) Eq (2.62) (phase-modulated lattice), (c) Eq (2.63) (multi-periodic lattice).

The trigonometric form of ψ_{12} gives a periodic lattice in x and z. The functions g_1, g_2, and g_3 shift and distort the lattice.

Case 2.4: Hyperbolic tangent kink profile

By applying $\rho_1 = \rho_2 = \rho_7 = 0$ and setting $\rho_3 = \rho_6 = \rho_8 = 1$, the reduced system simplifies to:

$$\Omega(\varphi, \zeta) = \frac{6\varepsilon_1 \tanh(\varphi)}{\beta} - \frac{\left(4\varepsilon_1^3 + 1\right)\zeta}{\beta\varepsilon_2\varepsilon_1}. \tag{2.64}$$

Substituting these conditions back into Eq (2.51) yields:

$$\begin{aligned} &p(z,t) = 1, \qquad q(y,z,t) = \left(\frac{1-c_1}{\beta\varepsilon_1^2}\right)y + g_1(z,t), \\ &\theta(y,t) = c_1 t + y, \qquad \eta(z,t) = c_2 t + \frac{(c_2\varepsilon_1 - 2\varepsilon_2(c_1-1))z}{\varepsilon_1^2}. \end{aligned} \tag{2.65}$$

Substituting these coefficients into the ansatz yields the hyperbolic tangent kink profile

$$\psi_{13}(x,y,z,t) = \frac{6\varepsilon_1}{\beta}\tanh(\varepsilon_1 x + c_1 t + y) - \frac{4\varepsilon_1^3 + 1}{\beta\,\varepsilon_1\,\varepsilon_2}\left(\varepsilon_2 x + c_2 t + \frac{c_2\varepsilon_1 - 2\varepsilon_2(c_1-1)}{\varepsilon_1^2}\,z\right) + \frac{1-c_1}{\beta\,\varepsilon_1^2}\,y + g_1(z,t). \tag{2.66}$$

Case 2.5: Hyperbolic–exponential mixed wave solution

Considering the parameter choices $\rho_4 = 1$, $\rho_5 = \rho_6$, and $\rho_1 = \rho_2 = \rho_7 = 0$ yields the following reduction:

$$\Omega(\varphi, \zeta) = \left(c_1 e^{\frac{\varepsilon_1\zeta}{\varepsilon_2}} + c_2 e^{-\frac{\varepsilon_1\zeta}{\varepsilon_2}}\right)\sinh(\varphi) + \left(c_3 e^{\frac{\varepsilon_1\zeta}{\varepsilon_2}} + c_4 e^{-\frac{\varepsilon_1\zeta}{\varepsilon_2}}\right)\cosh(\varphi) + c_5\zeta. \tag{2.67}$$

Substituting these parameter values into Eq (2.51) gives:

$$p(z,t) = g_1(t), \qquad q(y,z,t) = -\frac{y}{\varepsilon_2\beta} + g_3(z,t), \qquad \theta(y,t) = g_2(t), \qquad \eta(z,t) = -2z + g_4(t). \tag{2.68}$$

Hence, the hyperbolic–exponential mixed wave solution to the modified EMC model is given by:

$$\begin{aligned}\psi_{14}(x,y,z,t) = g_1(t)\Bigg[&\left(c_1 e^{\frac{\varepsilon_1(\varepsilon_2 x-2z+g_4(t))}{\varepsilon_2}} + c_2 e^{-\frac{\varepsilon_1(\varepsilon_2 x-2z+g_4(t))}{\varepsilon_2}}\right)\sinh\left(\varepsilon_1 x + g_2(t)\right)\\ &+\left(c_3 e^{\frac{\varepsilon_1(\varepsilon_2 x-2z+g_4(t))}{\varepsilon_2}} + c_4 e^{-\frac{\varepsilon_1(\varepsilon_2 x-2z+g_4(t))}{\varepsilon_2}}\right)\cosh\left(\varepsilon_1 x + g_2(t)\right) + c_5\left(\varepsilon_2 x - 2z + g_4(t)\right)\Bigg] - \frac{y}{\varepsilon_2\beta} + g_3(z,t).\end{aligned} \tag{2.69}$$

Case 2.6: Exponentially modulated background wave solution

Assuming the constraints $\rho_2 = \rho_5$, $\rho_6 = 0$, and $\rho_3 = \rho_4 = \rho_8$, the reduced system becomes:

$$\Omega(\varphi,\zeta) = \exp\left(\varphi - \frac{\varepsilon_1}{\varepsilon_2}\zeta\right) - \frac{\varepsilon_1}{\varepsilon_2}\zeta. \tag{2.70}$$

Further, Eq (2.51) yields

$$\begin{aligned}&p(z,t) = \beta\varepsilon_1^2\, g_3\Big(\frac{\beta t\varepsilon_1^3 - z}{\beta\varepsilon_1^3}\Big), \qquad q(y,z,t) = g_3\Big(\frac{\beta t\varepsilon_1^3 - z}{\beta\varepsilon_1^3}\Big)y + g_2(z,t),\\ &\theta(y,t) = g_1(t), \qquad \eta(z,t) = -\beta(\varepsilon_1^2 - \varepsilon_2)\int g_3\Big(\frac{\beta t\varepsilon_1^3 - z}{\beta\varepsilon_1^3}\Big)dz + g_4(t).\end{aligned} \tag{2.71}$$

Hence, an exponentially modulated background wave solution to the model is given by:

$$\begin{aligned}\psi_{15}(x,y,z,t) = \beta\varepsilon_1^2\, g_3\left(\frac{\beta t\varepsilon_1^3 - z}{\beta\varepsilon_1^3}\right)\Bigg[&-\varepsilon_1 x + \frac{\varepsilon_1}{\varepsilon_2}\beta(\varepsilon_1^2 - \varepsilon_2)\int g_3\left(\frac{\beta t\varepsilon_1^3 - z}{\beta\varepsilon_1^3}\right)dz - \frac{\varepsilon_1}{\varepsilon_2}g_4(t)\\ &+\exp\left(g_1(t) + \frac{\varepsilon_1}{\varepsilon_2}\beta(\varepsilon_1^2 - \varepsilon_2)\int g_3\left(\frac{\beta t\varepsilon_1^3 - z}{\beta\varepsilon_1^3}\right)dz - \frac{\varepsilon_1}{\varepsilon_2}g_4(t)\right)\Bigg] + g_3\left(\frac{\beta t\varepsilon_1^3 - z}{\beta\varepsilon_1^3}\right)y + g_2(z,t).\end{aligned} \tag{2.72}$$

Remark 3. This study has several limitations. The ansatz $\psi = p\Lambda + q$ with one or two phases covers only the cases in which the reduced equations (2.3) and (2.50) can be solved, and it does not yield well-known solution types such as multi-soliton or lump solutions. Since the paper is primarily concerned with analytical techniques, the constraints on the ρ_i were selected to ensure mathematical solvability rather than to reflect physical considerations.

Remark 4. It is also notable that Eq (1.9) is invariant under $\psi \to \psi + C(z,t)$.

Remark 5. All solutions obtained in this study have been verified through direct substitution into the modified EMC equation (1.9) using Maple.

3. Graphical discussion and behavior of the solutions

This section provides graphical discussion of the exact wave solutions derived in the previous section.

3.1. *Superposition of two counter-propagating pulses in ψ_1*

In this subsection, we investigate the spatial structure and crossing dynamics of the exact wave solution $\psi_1(x, y, z, t)$ with $\varepsilon = \beta = 1$, and the seed functions:

$$\begin{aligned} &h_1(t) = 0, \quad h_2(t) = 0, \quad g_4(t) = 0, \quad g_2(z,t) = 0, \quad g_1(z,t) = 0.7\text{sech}^2(0.8z), \\ &g_3(\xi,t) = 2.2\left[\text{sech}^2(\xi - 1.2t) + \text{sech}^2(\xi + 1.2t)\right]. \end{aligned} \tag{3.1}$$

Figure 8 illustrates the spatiotemporal dynamics of $\psi_1(x, 1, z, t)$ across the domain $[-7, 7] \times [-7, 7]$ at $t = -2, 0, 2$. At $t = -2$ (Figure 8(a)), two counter-propagating sech^2 pulses whose crests lie on the curves $\xi = \pm 1.2t$, where $\xi = \beta \int g_1(z,t)\, dz + x$; the z-dependence of ξ bends the wave fronts. At $t = 0$ (Figure 8(b)), the two pulses overlap along the curve $\xi = 0$, and the peak reaches $2 \times 2.2 = 4.4$ above the background ridge. At $t = 2$ (Figure 8(c)), they separate again with their original shape and amplitude, while the ridge $g_1(z)$ is unchanged.

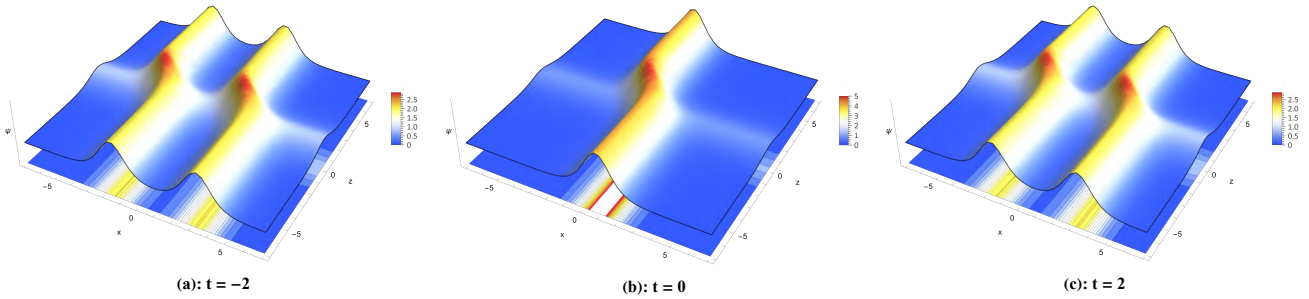


Figure 8. Dynamic evolution of $\psi_1(x, 1, z, t)$ evaluated at (a) $t = -2$, (b) $t = 0$, and (c) $t = 2$ with parameters $\varepsilon = \beta = 1$.

3.2. *One-dimensional wave dynamics and slice profiles of ψ_2*

To examine the temporal oscillation and spatial localization of ψ_2, we consider the exact wave profiles across Cases **(a)** and **(b)** as previously defined by Eqs (2.13) and (2.14), respectively. Figure 9 illustrates representative one-dimensional slice profiles.

3.3. *Some modulation effects in ψ_9*

In this subsection, we demonstrate the modeling flexibility of $\psi_9(x, y, z, t)$. To this end, $\Lambda(\varphi, t) = 4\,\text{sech}^2(\varphi)$, $g_2(z,t) = 0, g_4(t) = 1, g_5(t) = 0$ is considered. Moreover, we take $\varepsilon = \beta = 1$, and the following seed functions:

$$\begin{aligned} &\textbf{(a):} \quad g_1(z,t) = 0.9\, z\, e^{-0.15z^2} \sin(2t), \quad g_3(\xi,t) = -6\ \text{sech}^2(0.2\xi)\cos(1.5t) - 4\xi^2 e^{-0.1\xi^2}, \\ &\textbf{(b):} \quad g_1(z,t) = 2.5\ \text{sech}^2(z)\cos(2t), \quad g_3(\xi,t) = -5\sin^2(3\xi)\,\text{sech}(0.5t) - 3\cos(4\xi)e^{-0.1\xi^2}, \\ &\textbf{(c):} \quad g_1(z,t) = \frac{3}{1+z^2}\cos(t), \quad g_3(\xi,t) = 4\cos(5\xi)\cos(5t)e^{-0.05(\xi^2+t^2)} - 3\,\text{sech}^2(0.3(\xi - t)). \end{aligned} \tag{3.2}$$

Figure 10 illustrates the three-dimensional surface profiles and floor-projected contours of $\psi_9(1, 1, z, t)$ over the (z, t) domain.

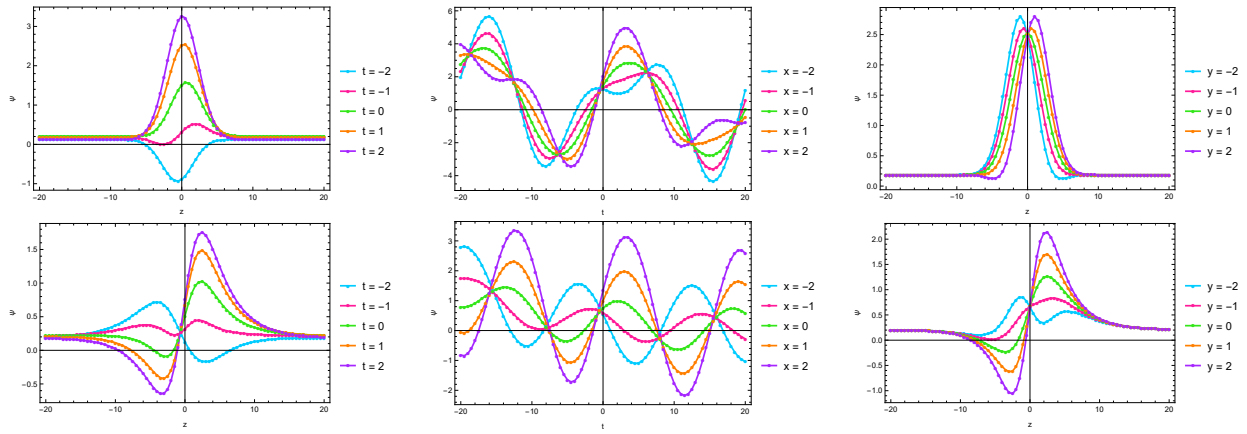


Figure 9. One-dimensional slice profiles of wave solution ψ_2: the first row corresponds to Case (a) in (2.13), and the second row corresponds to Case (b) in (2.14) with the remaining coordinates fixed to unity.

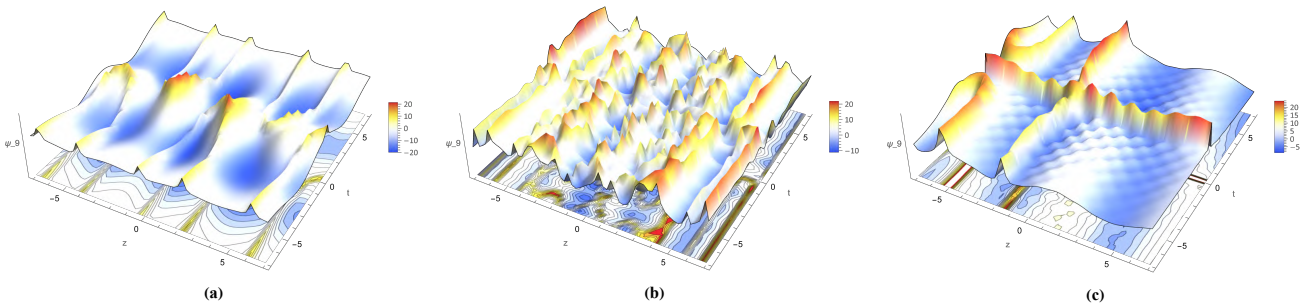


Figure 10. Dynamic evolution of $\psi_9(1, 1, z, t)$ using the seed functions (3.2).

3.4. Dynamic analysis and extreme–value evaluation for ψ_{11}

To construct localized rational-pulse profiles for $\psi_{11}(x, y, z, t)$, the seed function $g_1(z, t)$ is taken to be a time-dependent superposition of rational functions:

$$g_1^{(M)}(z,t) = c_0^{(M)} + \sum_{i=1}^{M} \frac{\sigma_i}{\omega_i + (l_i z - v_i t - b_i)^2}, \tag{3.3}$$

where M is the number of rational pulses, $c_0^{(M)}$ is a constant, l_i is a spatial scaling factor, v_i is the longitudinal velocity, b_i is the spatial phase shift, while σ_i and ω_i represent the weight coefficient and shape parameter of the i-th pulse, respectively.

In what follows, we investigate the dynamic behavior and extremum characteristics for $M = 1$ and $M = 2$, with $\varepsilon_1 = 0.8$, $\varepsilon_2 = 1, \beta = 1.2$, along with $g_2(y) = 2/(0.8 + y^2)$ evaluated at the snapshot $x_0 = 0$ and $t_0 = 0$.

Single-pulse configuration ($M = 1$): For the single-pulse state, the seed function reduces to:

$$g_1^{(1)}(z,t) = c_0^{(1)} + \frac{\sigma_1}{\omega_1 + (l_1 z - v_1 t - b_1)^2}. \tag{3.4}$$

For $c_0^{(1)} = 0.1$, $\sigma_1 = 1.5$, $\omega_1 = 0.4$, $l_1 = 1, v_1 = 0.7, b_1 = 0$ in (3.4), and restricting $\psi_{11}^{(1)}(x, y, z, t)$ to $x = 0$, $t = 0$ gives the scalar field $U(y, z)$. Setting $\nabla_{(y,z)}U = \mathbf{0}$ yields a critical point at $P_1(0, 0)$. At this point, the corresponding Hessian matrix is given by:

$$H(P_1) \approx \begin{pmatrix} -7.605 & 0 \\ 0 & -18.75 \end{pmatrix}, \quad \det H(P_1) \approx 142.6 > 0. \tag{3.5}$$

Given $\det H(P_1) > 0$ and both Hessian eigenvalues are negative, P_1 is a local maximum with a peak amplitude of $\psi_{\max} \approx 6.16$.

Superposition of rational pulses configuration ($M = 2$): In this case, we have

$$g_1^{(2)}(z, t) = c_0^{(2)} + \frac{\sigma_1}{\omega_1 + (l_1 z - v_1 t - b_1)^2} + \frac{\sigma_2}{\omega_2 + (l_2 z - v_2 t - b_2)^2}. \tag{3.6}$$

Let us fix the parameters $c_0^{(2)} = 0.3$, $\sigma_1 = 0.5$, $\omega_1 = 0.6$, $l_1 = 0.80$, and $v_1 = 0.4$, $\sigma_2 = 2, \omega_2 = 0.8, l_2 = 0.3, b_1 = 1.4, b_2 = -1.4, v_2 = 0.7$ in (3.6), and define $W(y, z) = \psi_{11}(x_0, y, z, t_0)$. Then, solving $\nabla_{(y,z)}W = \mathbf{0}$ yields the following three critical points:

The local maximum point $P_1 \approx (0, -4.66)$: At this point, the Hessian matrix is evaluated as:

$$H(P_1) = \begin{pmatrix} -7.61 & 0 \\ 0 & -0.56 \end{pmatrix}, \quad \det H(P_1) \approx 4.26 > 0. \tag{3.7}$$

Given $\det H(P_1) > 0$ and negative principal curvatures, P_1 is a local maximum with a peak amplitude of $W(P_1) \approx 5.13$.

The local maximum point $P_2 \approx (0, 1.68)$: This point satisfies the same conditions and is therefore another local maximum with a peak amplitude of $W(P_2) \approx 3.89$.

The saddle point $P_s \approx (0, 0.16)$: At the critical point P_s, we have $\det H(P_s) < 0$, making it a saddle point with a value of $W(P_s) \approx 3.53$. The graphical representations of these cases are displayed in Figures 11 and 12.

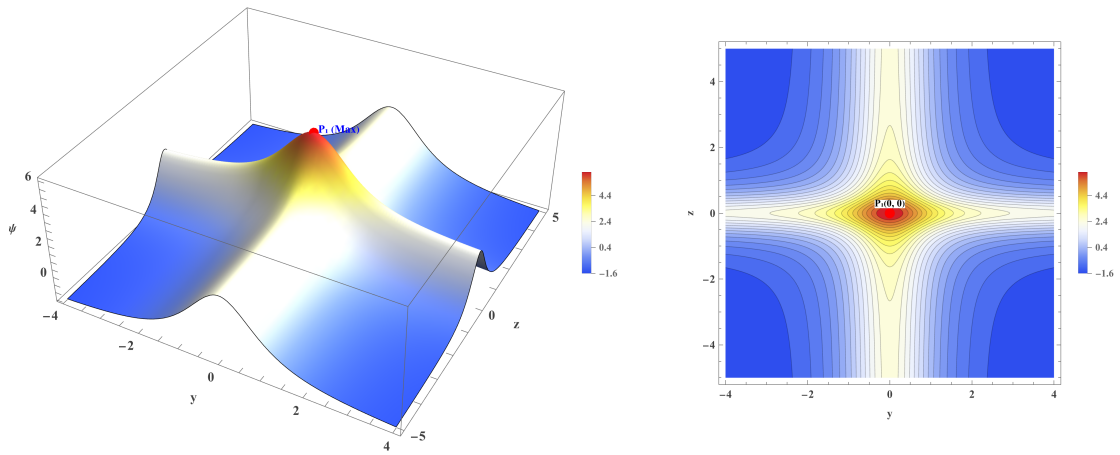


Figure 11. Extremum analysis and critical point classification of ψ_{11} for the single-pulse configuration (3.4).

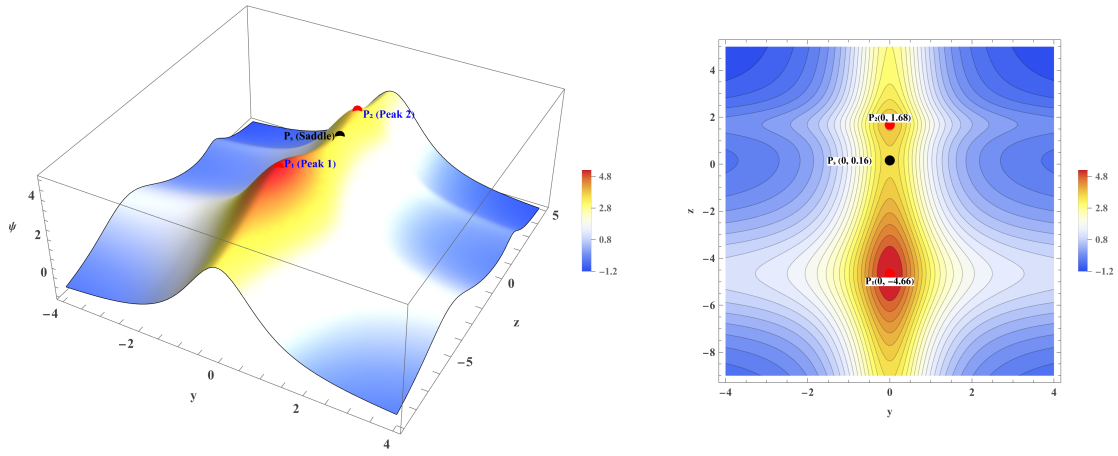


Figure 12. Extremum analysis and critical point classification of ψ_{11} for the multi-pulse configuration (3.6).

3.5. Parameter sensitivity analysis of ψ_{11} and ψ_{12}

Sensitivity analysis serves to identify and quantify the impact of parameter variations on the resulting wave solutions. In this subsection, we analyze the sensitivity of ψ_{11} and ψ_{12} to parameter variations. Figure 13 presents the impact of the parameters ε_1, ε_2, and β on the solution ψ_{11} with $g_1(z,t) = 0, g_2(y) = \sin y$ at $x = 0, z = 0, t = 1$. Similarly, Figure 14 depicts the impact of ε_1, ε_2, and β on ψ_{12} for $g_1(t) = 0, g_2(z,t) = \sin(z+t)$, and $g_3(t) = t$ at $x = 0, y = 1, z = 0$.

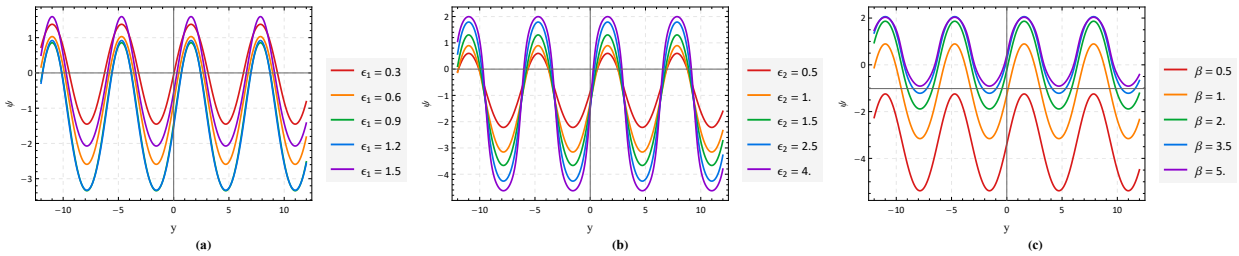


Figure 13. Two-dimensional profile of ψ_{11} along the y-axis. The non-swept parameters are fixed at $(\varepsilon_1, \varepsilon_2, \beta) = (0.8, 1, 1)$, while the swept parameters take the values $\varepsilon_1 \in \{0.3, 0.6, 0.9, 1.2, 1.5\}$ (a), $\varepsilon_2 \in \{0.5, 1, 1.5, 2.5, 4\}$ (b), and $\beta \in \{0.5, 1, 2, 3.5, 5\}$ (c).

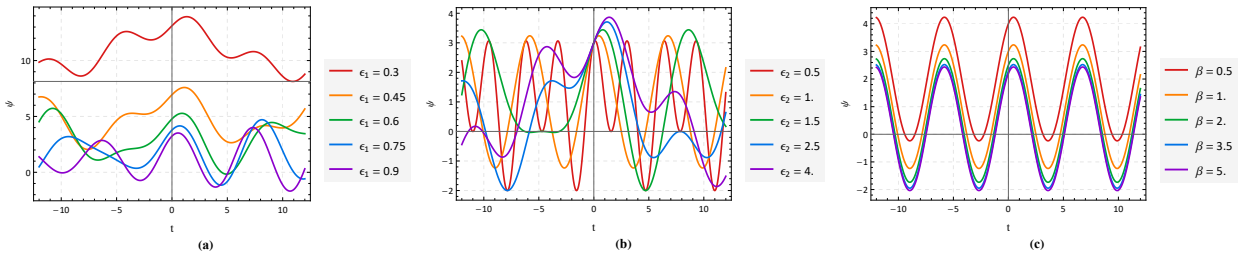


Figure 14. Two-dimensional profile of ψ_{12} along the t-axis. The non-swept parameters are fixed at $(\varepsilon_1, \varepsilon_2, \beta) = (1, 1, 1)$, while the swept parameters take the values $\varepsilon_1 \in \{0.3, 0.45, 0.6, 0.75, 0.9\}$ (a), $\varepsilon_2 \in \{0.5, 1, 1.5, 2.5, 4\}$ (b), and $\beta \in \{0.5, 1, 2, 3.5, 5\}$ (c).

3.6. *Solitary structures in ψ_{11} and ψ_{13}*

The functions ψ_{11} and ψ_{13} contain a hyperbolic step in x added to a part that is linear in x, so that ψ itself is a kink on a ramp. Differentiating Eq (2.66) gives

$$\partial_x\psi_{13} = \frac{6\varepsilon_1^2}{\beta}\,\mathrm{sech}^2\left(\varepsilon_1 x + c_1 t + y\right) - \frac{4\varepsilon_1^3 + 1}{\beta\varepsilon_1}, \tag{3.8}$$

and differentiating Eq (2.57) gives

$$\partial_x\psi_{11} = \frac{3\varepsilon_1^2}{2\beta}\,\mathrm{sech}^2\left(\frac{\vartheta}{2}\right) - \frac{\varepsilon_1^2}{\beta}, \qquad \vartheta = \varepsilon_1\Big(x - \frac{\varepsilon_1}{\varepsilon_2}t\Big) + \beta\varepsilon_2\, g_2(y). \tag{3.9}$$

Both are sech^2 pulses on a constant pedestal. Taking the pulse as $A\,\mathrm{sech}^2(s/w)$, where s is the coordinate across the crest, the following quantities can be read off. ψ_{13}*:* amplitude $A = 6\varepsilon_1^2/\beta$, width $w = 1/\varepsilon_1$, crest on the line $\varepsilon_1 x + c_1 t + y = 0$ of the (x, y)-plane, which moves in the x-direction with velocity $-c_1/\varepsilon_1$, and integral across the pulse $12\varepsilon_1/\beta$. ψ_{11}*:* amplitude $A = 3\varepsilon_1^2/(2\beta)$, width $w = 2/\varepsilon_1$, crest at $x = (\varepsilon_1/\varepsilon_2)t - (\beta\varepsilon_2/\varepsilon_1)g_2(y)$, velocity $\varepsilon_1/\varepsilon_2$, and integral across the pulse $6\varepsilon_1/\beta$. In both cases $\beta A w^2 = 6$, so that the amplitude is fixed by the width and by β. The arbitrary function $g_2(y)$ of ψ_{11} does not change the amplitude, the width, or the velocity. It changes only the shape of the crest in the (x, y)-plane, which is the curve $x = -(\beta\varepsilon_2/\varepsilon_1)g_2(y)$ at $t = 0$. The crest of ψ_{13} is a straight line in the (x, y)-plane for every t. The fields (3.8) and (3.9) do not depend on z, and the function $g_1(z, t)$ enters ψ_{11} and ψ_{13} only additively. Figure 15 (a) and (b) show $\partial_x\psi_{13}$ and $\partial_x\psi_{11}$.

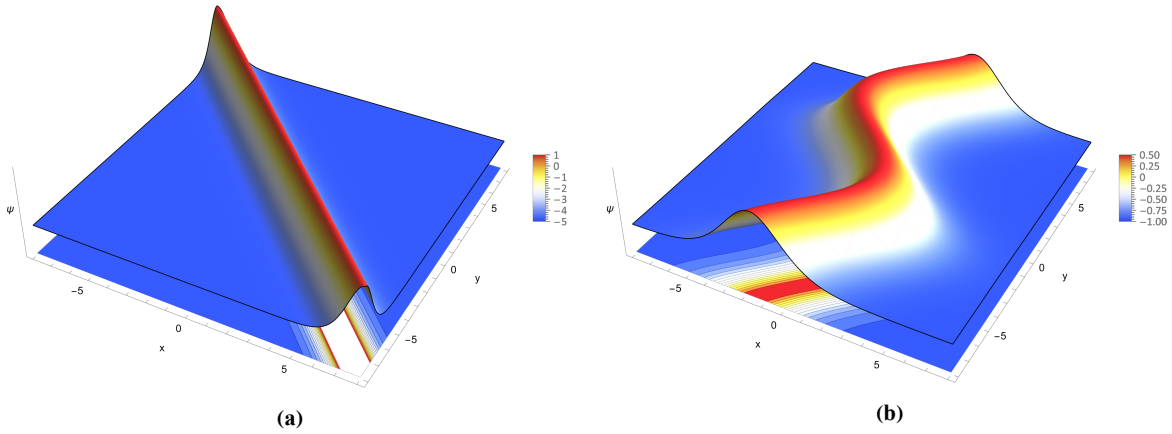


Figure 15. (a) $\partial_x\psi_{13}$ at $t = 0$ with $c_1 = 1$ and $\varepsilon_1 = \beta = 1$; (b) $\partial_x\psi_{11}$ at $t = 0$ with $\varepsilon_1 = \varepsilon_2 = \beta = 1$ and $g_2(y) = 2\sin(0.5y)$. Both are shown in the (x, y)-plane.

4. Conclusions

In this paper, we have developed an analytic framework to construct diverse classes of non–traveling wave solutions to the modified (3 + 1)–dimensional EMC equation. To this end, we adopted two extended variable-separation reduction strategies to simplify the governing Eq (1.9), yielding the more tractable reduced forms (2.3) and (2.50). Then, by imposing various algebraic constraints on these reductions, several families of explicit exact solutions were obtained. The first

reduction involves one mixed phase, is more direct, and yields closed-form non–traveling solutions with free functions. This reduction strategy leads to solutions of linear, parabolic-exponential, quadratic-background, exponential-decay, and unconstrained functional types. The second reduction, on the other hand, uses two independent phases and has more structural flexibility, resulting in additional solution families with a stronger multi-phase coupling mechanism. From this reduction strategy, various exponential linear background, logistic step, trigonometric lattice, hyperbolic tangent and mixed hyperbolic–exponential solutions were determined. We note that many existing studies concern the original (1+1)-dimensional EMC equation (1.6) and its fractional or generalized variants, not the modified (3 + 1)–dimensional equation (1.9); our solutions can therefore be compared with those in the literature via the reductions of (1.9) to (1.8) and (1.6). Among the solutions obtained, ψ_9 provides a general family of non–traveling wave solutions. We also provide a graphical discussion of the exact solutions, including the effects of selected seed functions and parameters on their behavior. The technique used in this paper can be viewed as an efficient analytical tool for studying other nonlinear models in fluid dynamics. One possible future direction for this work involves investigating fractional-order versions of the EMC equation using fractal derivatives to model wave propagation in media with non-smooth boundaries [25, 26].

Author contributions

Zhi-Hua Bao: Software, validation, methodology, conceptualization; Shami A. M. Alsallami: Methodology, visualization, validation, writing–original draft, conceptualization. All authors have read and approved the final version of the manuscript for publication.

Use of Generative-AI tools declaration

The authors declare they have not used Artificial Intelligence (AI) tools in the creation of this article.

Conflict of interest

The authors declare that they have no conflict of interest in this paper.

References

1. H. P. McKean, Boussinesq's equation on the circle, *Commun. Pure Appl. Math.*, **34** (1981), 599–691. https://doi.org/10.1002/cpa.3160340502
2. M. Matsukawa, S. Watanabe, N-soliton solution of two dimensional modified Boussinesq equation, *J. Phys. Soc. Jpn.*, **57** (1988), 2936–2940. https://doi.org/10.1143/JPSJ.57.2936
3. R. S. Johnson, A modern introduction to the mathematical theory of water waves, Cambridge: Cambridge University Press, 1997.
4. A. Biswas, D. Milovic, A. Ranasinghe, Solitary waves of Boussinesq equation in a power law media, *Commun. Nonlinear Sci.*, **14** (2009), 3738–3742. https://doi.org/10.1016/j.cnsns.2009.02.021

5. M. Dehghan, R. Salehi, A meshless based numerical technique for traveling solitary wave solution of Boussinesq equation, *Appl. Math. Model.*, **36** (2012), 1939–1956. https://doi.org/10.1016/j.apm.2011.07.075
6. G. ur Rahman, Abdullah, M. Z. Meetei, J. F. Gómez-Aguilar, Investigation of the dynamical perspective of soliton solutions to the (3+1)-dimensional Boussinesq model using two distinctive methods, *Nonlinear Dyn.*, **113** (2025), 25097–25119. https://doi.org/10.1007/s11071-025-11398-4
7. J. V. Boussinesq, Essai sur la théorie des eaux courantes, *Mémoires Présentés par Divers Savants à l'Académie des Sciences*, 1877.
8. A. M. Wazwaz, L. Kaur, New integrable Boussinesq equations of distinct dimensions with diverse variety of soliton solutions, *Nonlinear Dyn.*, **97** (2019), 83–94. https://doi.org/10.1007/s11071-019-04955-1
9. M. Inc, New solitary wave solutions with compact support and Jacobi elliptic function solutions for the nonlinearity dispersive Boussinesq equations, *Chaos Soliton. Fract.*, **37** (2008), 792–798. https://doi.org/10.1016/j.chaos.2006.09.064
10. K. S. Nisar, R. Silambarasan, Jacobi elliptic solutions, bright, compound bright-complex singular solitons of (3+1)–dimensional Wazwaz Kaur Boussinesq equation, *Opt. Quant. Electron.*, **56** (2024), 1301. https://doi.org/10.1007/s11082-024-07213-w
11. E. L. Mansfield, P. A. Clarkson, Symmetries and exact solutions for a 2+1-dimensional shallow-water wave equation, *Math. Comput. Simulat.*, **43** (1997), 39–55. https://doi.org/10.1016/S0378-4754(96)00054-7
12. H. Qawaqneh, Y. Alrashedi, Mathematical and physical analysis of fractional Estevez–Mansfield–Clarkson equation, *Fractal Fract.*, **8** (2024), 467. https://doi.org/10.3390/fractalfract8080467
13. J. Muhammad, N. Nasreen, E. Hussain, U. Younas, A. S. Alsubaie, On the study of analytical soliton solutions and interaction aspects to the Estevez–Mansfield–Clarkson equation arising in diversity of fields, *Phys. Scr.*, **99** (2024), 115221. https://doi.org/10.1088/1402-4896/ad804b
14. M. Alqudah, S. Mukhtar, H. A. Alyousef, S. M. E. Ismaeel, S. A. El-Tantawy, F. Ghani, Probing the diversity of soliton phenomena within conformable Estevez–Mansfield–Clarkson equation in shallow-water, *AIMS Mathematics*, **9** (2024), 21212–21238. https://doi.org/10.3934/math.20241030
15. M. M. Al-Sawalha, S. Noor, S. Alshammari, A. H. Ganie, A. Shafee, Analytical insights into solitary wave solutions of the fractional Estevez–Mansfield–Clarkson equation, *AIMS Mathematics*, **9** (2024), 13589–13606. https://doi.org/10.3934/math.2024663
16. A. I. Aliyu, J. S. Yusuf, M. M. Nauman, D. U. Ozsahin, B. G. Agaie, J. H. Zaini, et al., Lie symmetry analysis and explicit solutions to the Estevez–Mansfield–Clarkson equation, *Symmetry*, **16** (2024), 1194. https://doi.org/10.3390/sym16091194
17. G. H. Tipu, W. A. Faridi, F. Yao, M. Garayev, Uncovering nonlinear dynamics in shallow-water: an analytic approach to the (1+1)-dimensional Estevez–Mansfield–Clarkson equation, *J. Ocean Eng. Mar. Energy*, **11** (2025), 799–818. https://doi.org/10.1007/s40722-025-00401-0

18. Y. Zhang, X. Xie, X. Gong, X. Xin, Soliton solutions and lump solutions of the generalized multi-dimensional Estevez–Mansfield–Clarkson equation with time-varying coefficients, and learning of the equation based on augmented GPINN, *Phys. Scr.*, **101** (2026), 315206. https://doi.org/10.1088/1402-4896/ae8343

19. N. Ahmed, J. E. Macías-Díaz, S. Umer, M. Z. Baber, M. Jawaz, H. Vargas-Rodríguez, On some solitary wave solutions of the Estevez–Mansfield–Clarkson equation with conformable fractional derivatives in time, *Open Phys.*, **22** (2024), 20240109. https://doi.org/10.1515/phys-2024-0109

20. Z. Y. Yan, Abundant symmetries and exact compacton-like structures in the two-parameter family of the Estevez–Mansfield–Clarkson equations, *Commun. Theor. Phys.*, **37** (2002), 27. https://doi.org/10.1088/0253-6102/37/1/27

21. Y. Zhang, X. Gong, X. Xie, X. Xin, Soliton and lump solutions of the Estevez–Mansfield–Clarkson equation and learning the equation based on extended GPINN, *Pramana*, **100** (2026), 104. https://doi.org/10.1007/s12043-026-03137-0

22. B. Ceesay, M. Z. Baber, T. A. Sulaiman, M. Bayram, W. W. Mohammed, H. Emadifar, et al., Exact soliton and interaction solutions of the Estevez–Mansfield–Clarkson equation, *Results Eng.*, **29** (2026), 109174. https://doi.org/10.1016/j.rineng.2026.109174

23. S. A. M. Alsallami, On exact non–traveling wave solutions to the generalized nonlinear Kadomtsev–Petviashvili equation in plasma physics and fluid mechanics, *Mathematics*, **13** (2025), 1914. https://doi.org/10.3390/math13121914

24. S. A. M. Alsallami, Investigating exact solutions for the (3+1)-dimensional KdV-CBS equation: A non–traveling wave approach, *AIMS Mathematics*, **10** (2025), 6853–6872. https://doi.org/10.3934/math.2025314

25. Y. Sun, J. F. Lu, Variational approach for the fractal generalized Bogoyavlensky–Konopelchenko equation, *Therm. Sci.*, **30** (2026), 837–846. https://doi.org/10.2298/TSCI2602837S

26. J. Lu, Application of variational principle and fractal complex transformation to (3+1)-dimensional fractal potential-YTSF equation, *Fractals*, **32** (2024), 2450027. https://doi.org/10.1142/S0218348X24500270



AIMS Press

© 2026 the Author(s), licensee AIMS Press. This is an open access article distributed under the terms of the Creative Commons Attribution License (https://creativecommons.org/licenses/by/4.0)